Universitat
de les Illes Balears

Dynamics of attracting Brownian particles

Adrián García Candel

Master's Thesis

Master's degree in Physics on Complex Systems

at the

UNIVERSITAT DE LES ILLES BALEARS

Academic year: 2015-2016

Date 24/07/2017

UIB Master's Thesis Supervisor: Cristóbal López Sánchez

UIB Master's Thesis Co-Supervisor: Emilio Hernández-García

Abstract

We have studied the properties of an assembly of Brownian particles interacting via an attractive soft-core GEM-α potential in 1d. Through numerical simulations we show that the particles tend to aggregate in clusters that collapse at extremely long times. We determine the diffusion coefficient of the cluster formed and its dependencies. We perform a linear stability analysis of the system, finding the conditions that lead to a cluster formation. Also, by the study of the deterministic part of the equation for the macroscopic density we propose a relationship between the size of the cluster and the parameters of the potential and the particles. Through numerical simulations we check these results.

Acknowledgements

I would like to express my gratitude to my supervisors, Emilio Hernández-García and Cristóbal López for their help along this trip.

Many thanks to the Zulo's team and all the IFISC crew.

Gracias a mi familia por el apoyo incondicional a lo largo de toda esta etapa y todas las anteriores.

Gracias a Irene por su infinita paciencia y sus constantes mensajes de ánimo.

Contents

Chapter 1

Introduction

Brownian motion was described for the first time by Robert Brown in 1827 while he was observing pollen grains in water. He observed that the particles were moving randomly when they were suspended in a fluid, apparently without explanation. The mechanism behind that irregular motion was given by A. Einstein [1], who found that the cause of that erratic movement were the thermal molecular motions. Since then, Brownian motion has been applied in a large number of systems as a tool for modelling nature, from biological [2, 3] to social [4] systems.

Pattern formation for random walkers has been studied in many cases, for example in competition systems [5]. On the other hand [6] studied the pattern formation for discrete Brownian particles with repulsive soft-core interactions. This kind of repulsive soft-core potential appears in the context of soft matter, such as colloidal or polymeric systems, or even in biology where organisms do aggregate although they compete for the same resources. That study showed how clustering patterns can arise with repulsive interactions between an assembly of particles under thermal agitation, which seems counterintuitive. Using numerical simulations and analyzing the integro-differential Dean-Kawasaki [7] equation for the density of particles by performing a linear stability analysis, [6] explained the mechanism under that aggregation process both in 1 and 2d.

The central objective of this work is to analyze the dynamics of Brownian soft-core particles under an attractive potential in the overdamped limit. This completes previous results for the repulsive case. First, in Chapter 2 we will set the theory needed in order to study our model, which will be implemented in Chapter 3. While Section 2.1 will review the dynamics of our

systems, in Section 3.2 we will set the Dean-Kawasaki equation needed in further sections. On the other hand, Section 3.1 will show some preliminar results i.e. spatiotemporal trajectories of the proposed model; in Section 3.2 we will perform a linear stability analysis in order to study the robustness of the patterns formed by the attracting potential. Since the attractive force between particles is expected to make the particles collapse into a unique cluster, in Chapter 4 we will focus on determine the cluster properties such as its diffusion coefficient at Section 4.1, size in Section 4.2, both analytically in Section 4.2.1 and numerically in Section 4.2.2, and its critical transition point in Section 4.3. For simplicity we will focus on the one-dimensional system but the analysis is generalizable.

Attractive forces appear in particular in self-gravitating systems. In our case a system that could be modelled with soft-core attractive Brownian particles, we briefly introduce the Collembola clustering obsevations. Collembola, also called springtails, are one of the most widespread terrestial hexapods in the world, with over 6500 species described in the literature [8]. Collembola, under some conditions, tend to aggregate in the soil [9]. While some experimental studies were done [10], there's no a model that explains the mechanism of Collembola's aggregation. Comparing the photographs of the Collembola's clusters in Figs. 1.1b and 1.1c are pretty similar to the observed in the attractive sof-core interactions briefly introduced in the final section of [6].

While a realistic modeling of the mechanisms under the aggregation of Springtails is out of the aim of this work and they are not shown to interact attractively, this shows an example of how clustering is observed in nature and it is a field of interesting physics.

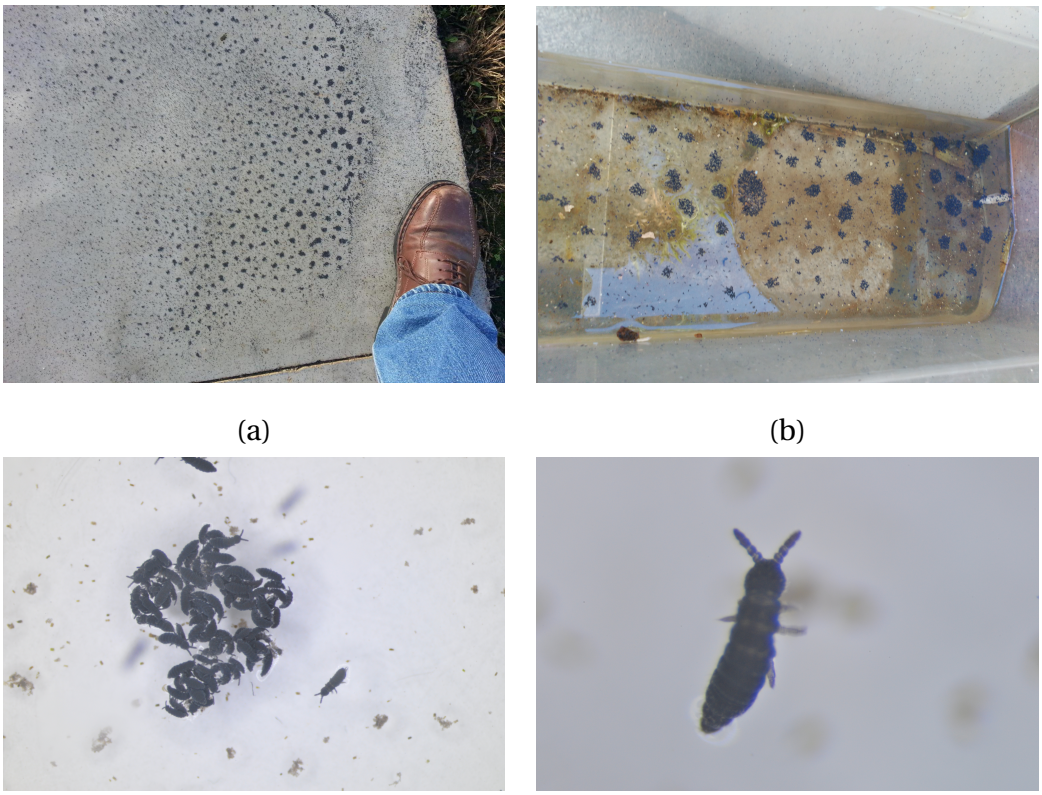

(a) (b)

(c) (d)

Figure 1.1: Photos of Collembola aggregations. (a) and (b) show how the Collembola form cluster patterns. (c) a close-up of one of the clusters, showing that is formed by aggregation of individuals. (c) a Collembola close-up of one individual taken from the clusters shown in (a), of the order Poduromorpha, family Hypogastruridae, *Hypogastrura collembola*. Photos taken on November, 2015 by (a) Emílio Hernández-Garcia, (b) Roberta Zambrini, (c) and (d) Miguel Ángel Miranda.

Chapter 2

System of particles and macroscopic description

2.1 Particle dynamics

In order to study the dynamics of the interacting Brownian particles we will set a model based on [6] where soft-core Brownian particles interact through a pairwise interaction potential.

We will consider the overdamped limit, where friction coefficient is γ and the N particles are exposed to Brownian motion subjected to a potential energy $U = \gamma V$, given by the

$$\dot{\vec{x}}_i = -\nabla_i V(\vec{x}_1, \vec{x}_2, ...\vec{x}_n) + \sqrt{2D}\vec{\xi}_i(t)\,,\; i = 1, ...N \tag{2.1}$$

where the random movement term is driven by the diffusion coefficient D given by the Einstein's relationship [11] $D = \frac{\kappa_B T}{\gamma}$, where κ_B the Boltzmann's constant, γ the friction coefficient and T the temperature of the system. ∇_i stands for the gradient with respect to the spatial coordinate $\vec{x}_i$. The random movement is given by Gaussian noise vectors that satisfy

$$\langle \vec{\xi}_i \rangle = 0, \tag{2.2}$$

$$\langle \vec{\xi}_i(t)\vec{\xi}_j(t') \rangle = \mathbb{1}\delta_{ij}\delta(t - t'), \tag{2.3}$$

where $\mathbb{1}$ is the d-dimensional identity matrix.

Assuming pairwise interactions i.e. $V(\vec{x}_1,...,\vec{x}_n) = \sum_{\langle ij\rangle} v(\vec{x}_i - \vec{x}_j)$, the equation (2.1) becomes

$$\dot{\vec{x}}_i = -\sum_{j=1}^{N} \nabla_i v(\vec{x}_i - \vec{x}_j) + \sqrt{2D}\vec{\xi}_i(t), \tag{2.4}$$

In order to model the interactions between the particles, we set a potential of the form

$$v(\vec{x}) \equiv \epsilon \exp\left(-\left|\frac{\vec{x}}{R}\right|^{\alpha}\right), \tag{2.5}$$

called GEM-α [12, 13] potential.

The soft-core refers to the fact that the potential does not diverge at $x = 0$, so the particles can overlap. R reflects the spatial range of the potential; at $x = R$ the potential strength decays to a factor $e^{-1} = 0.3679$ compared to the maximum value at $x = 0$. Our number of particles will be constant so we can define a system's mean density as $\rho_0 = \frac{N}{L^d}$ being N the number of particles and L^d the system's volume.

In order to impose attractive interactions, we set the restriction $\epsilon < 0$ to the magnitude of the potential. The force applied to the particles is defined as $\vec{F}(\vec{x}) = -\vec{\nabla} v(\vec{x})$ and it will be always negative i.e. attractive. This potential sets a family of functions whose profile gets more boxlike as the parameter α increases, as shown in Fig. 2.1.

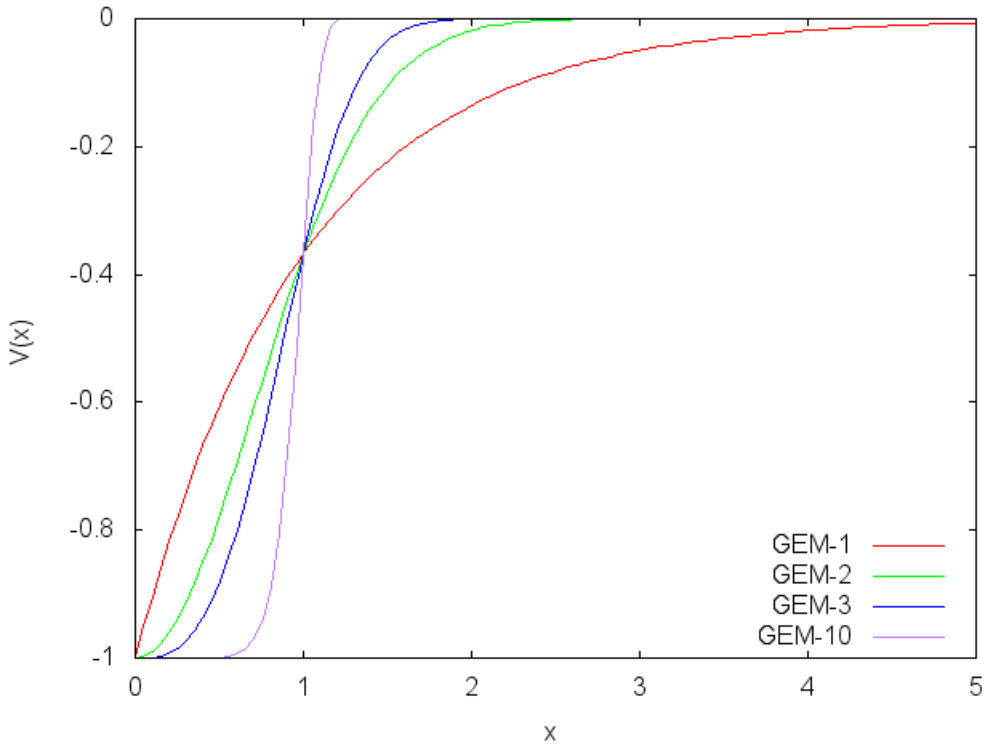

Figure 2.1: Profile of the GEM-α potential with all the other parameters set to 1. Red line is for $\alpha = 1$, green $\alpha = 2$, blue $\alpha = 3$ and purple $\alpha = 10$. Note that at $x = R = 1$ the magnitude of the potential has decreased more than the 50% of the maximum value.

Due to the familiarity with the Gaussian function we will focus on the case $\alpha = 2$ but the analysis could be generalized to any other value of α.

2.2 Dean-Kawasaki equation

For the theoretical analysis of the cluster we will use the Dean-Kawasaki equation [7] (DK) which is the stochastic equation followed by the density function for a systems of Langevin processes that interact through a pairwise potential. The DK equation gives the expected density evolution in the mean field approximation [7, 6, 14]. We will work with dimensionless variables $\tilde{D} = \frac{D}{\epsilon\rho_0 R}$, $\tilde{x} = \frac{x}{R}$, $\tilde{t} = t\rho_0\epsilon^{d-2}$, $\tilde{\rho}(\tilde{x},\tilde{t}) = \frac{\rho(x,t)}{\rho_0}$ and $\tilde{v} = \frac{v}{\epsilon}$, equivalent to set the parameters to $R = |\epsilon| = \rho_0 = 1$.

Using this notation the deterministic part of the Dean-Kawasaki equation [6] is

$$\partial_t \tilde{\rho}(\tilde{x}) = \nabla \cdot \left(\tilde{\rho}(\tilde{x}, \tilde{t}) \int dx' \nabla \tilde{v}(\tilde{x} - x') \tilde{\rho}(x', \tilde{t}) \right) + \tilde{D} \nabla^2 \tilde{\rho}(\tilde{x}, \tilde{t}), \tag{2.6}$$

which can be written as a particle conservation equation in the form

$$\frac{\partial \tilde{\rho}(\tilde{x}, \tilde{t})}{\partial \tilde{t}} = -\nabla \cdot J(\tilde{x}, \tilde{t}), \tag{2.7}$$

being $D\nabla^2 \rho(x,t)$ the diffusion term, and the flux

$$J(\tilde{x}, \tilde{t}) = -\tilde{\rho}(\tilde{x}, \tilde{t}) \int dx' \nabla \tilde{v}(\tilde{x} - x') \tilde{\rho}(\tilde{x}, \tilde{t}) - \tilde{D} \nabla \tilde{\rho}(\tilde{x}, \tilde{t}), \tag{2.8}$$

We will use this result in Section 4.2 to determine the relation between the potential parameters and the size of the cluster.

Chapter 3

Model results

3.1 Spatiotemporal dynamics

In order to integrate the stochastic differential equations (2.4) we will implement a Milstein scheme [15] while for the Gaussian noise a Box-Muller method [16] that gives two uncorrelated Gaussian random variables is used. We use periodic boundary conditions to the system to reduce finite system size effects. The distance between two particles will be determined as the minimum distance. This is justified for the short interaction range of the potential provided that $R \ll L$.

If the noise is small enough and we start from initial uniform distribution, the attractive potential will make the particles initially collapse in a number of clusters separated by a distance longer than R. That number of clusters will decrease as the diffusion and the attraction will reduce eventually the distance between clusters making them to collapse. As we can see in Fig. 2.1, the α parameter modulates the profile of the potential leading to different clustering dynamics of the Brownian particles as shown in Fig. 3.1.

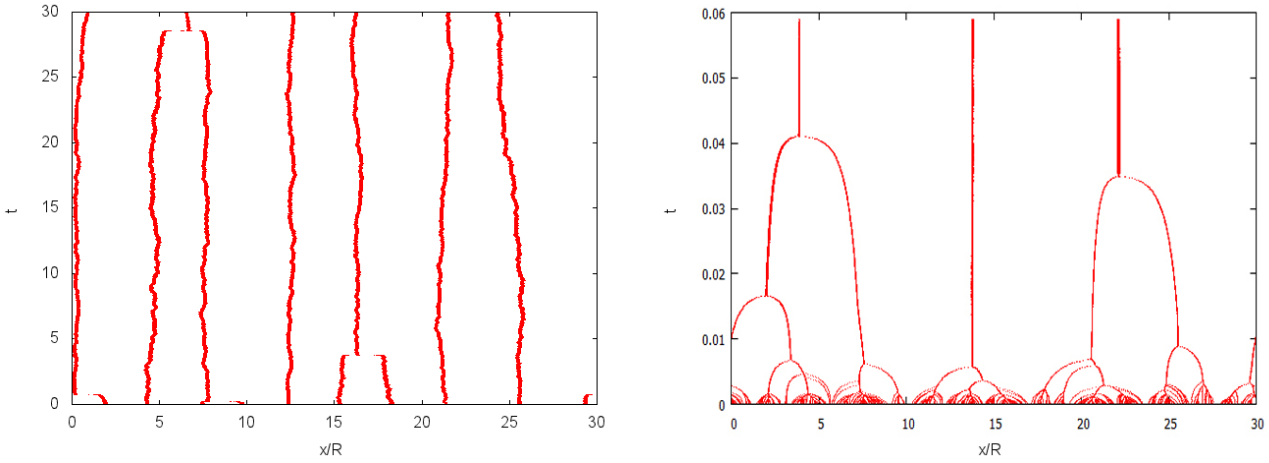

(a) (b)

Figure 3.1: Spatiotemporal dynamics for an assembly of particles from an initial random distribution. Time evolution is shown in y-axis while x-axis reflects the spatial distribution. (a) 600 particles with $\alpha = 1$, $R = 0.1$, $\rho_0 = 200$, $\epsilon = -0.33$, $L = 3$ and $D = 3.96 \times 10^{-3}$. (b) Same as (a) but $\alpha = 3$.

To have a better comparision we run the same simulation with the same random Gaussian numbers with different values of α as shown in Figs. 3.2. As we can see, the number of clusters at a certain time increases as α does. For example, for $t = 4$ there are only three clusters if $\alpha = 1$ while six clusters remain when $\alpha = 3$. That dependance of the number of clusters with α can be explained with the GEM-α profiles seen in Fig. 2.1. As α increases at a certain $x > R$ the strength of the potential will be smaller i.e. the tail of the potential is longer as α is smaller.

On the other hand, assuming that the particles are equally distributed among the clusters seems reasonable to think that the number of particles at each cluster will have a dependence on the parameter α. For the same ρ_0, the larger the number of clusters the fewer the number of particles at each cluster if we start with random initial conditions.

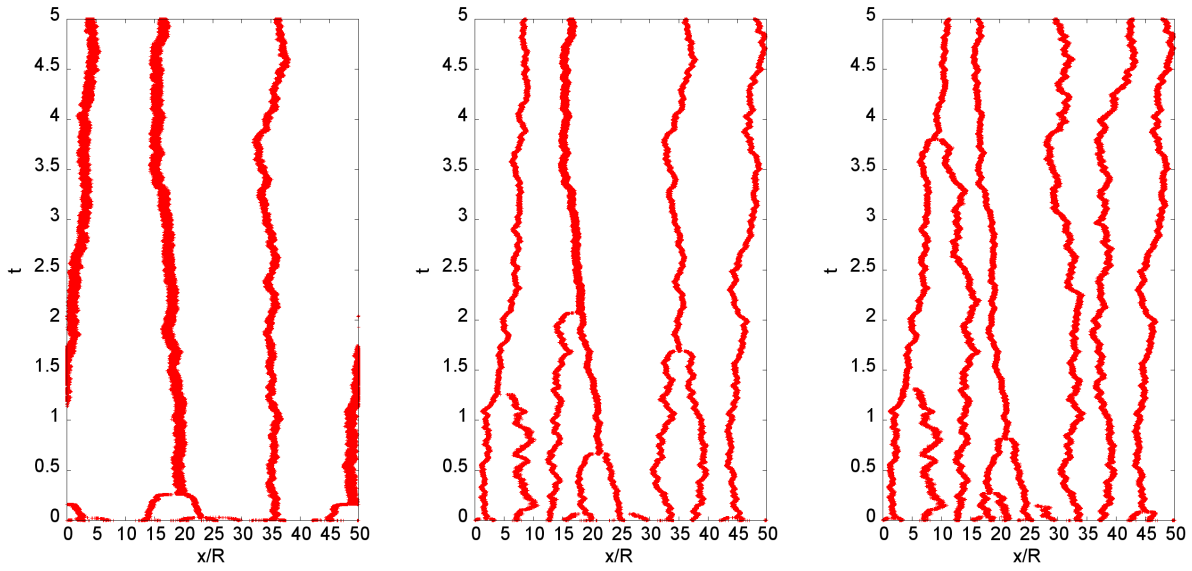

(a) (b) (c)

Figure 3.2: Dynamics of 100 Brownian particles with the same parameters except α. Time evolution is shown in y-axis while x-axis reflects the spatial distribution. $\rho_0 = 200$, $R = 0.01$, $\epsilon = -0.03$ and $D = 3 \times 10^{-3}$. The potential profile is determined by (a) $\alpha = 1$, (b) $\alpha = 2$ and (c) $\alpha = 3$.

Since we are considering an attracting potential, if the thermal noise is under a critical value all the Brownian particles will tend to collapse in an unique cluster. Actually, that will be the case at extremely long times providing we are in a cluster-formation situation, where the attraction is large enough to form aggregation. Due to the fast decay of the interaction strength, if distance between clusters is larger than R (and the diffussion coefficient is small) for not extremely long times they will be independent, and we can analyze the dynamics of the particles in an isolated cluster.

3.2 Linear stability analysis

We have seen how the clusters evolve in time and space but, why are clusters formed at all? In order to formulate a theory about the cluster formation we perform a linear stability analysis [6] around the homogeneous solution $\tilde{\rho}(\vec{x}) = \tilde{\rho}_0 = 1$. We will consider a small perturbation around the homogeneous solution of the form$\rho(\vec{x},t) = \rho_0 + \delta\rho(\vec{x},t)$ being $\delta\rho(\vec{x},t) = \exp\left(\lambda t + i\vec{k}\cdot\vec{x}\right)$. If we introduce that perturbation into the Dean-Kawasaki equation (2.6) we obtain the growth rate

$$\lambda(k) = -k^2 \left[\tilde{D} + \hat{v}(k)\right]. \tag{3.1}$$

Where the tilde stands for adimensional quantities as defined before. Being $\hat{v}(k)$ the Fourier transform of the potential, which is in the d-dimensional case

$$\hat{v}(\vec{k}) = \int \tilde{v}(\vec{x}) e^{-i\vec{k}\cdot\vec{x}} d\vec{x}. \tag{3.2}$$

Since we are only considering the 1-dimensional problem, $d = 1$ and all the vectorial quantities will be $|\vec{k}| = k$, $|\vec{x}| = x$. The clustering condition depends on (3.1). If we compare this growth rate with the one obtained for repulsive interactions studied in [5] we can see that the condition for clustering, as expected, is more robust for attractive interactions since the Fourier components are always negative, $\hat{v}(k) < 0$. In the repulsive case $\hat{v}(k)$ has negative Fourier components only for $\alpha > 2$. We have defined in Section the dimensionless potential $\tilde{v}(\tilde{x}) = \frac{v(x)}{\epsilon}$ so the GEM-α potential is expressed as

$$\tilde{v}(\tilde{x}) = -e^{-|\tilde{x}|^\alpha}. \tag{3.3}$$

In 1-d the Fourier transform of the potential is

$$\hat{v}(k) = \int \tilde{v}(x) e^{-ikx} dx. \tag{3.4}$$

An example of the growth rate (3.1) is plotted in Fig. 3.3 for different values of the diffusion coefficients and $\alpha = 2$. Positive values of $\lambda(k)$ means that the perturbation will grow if the system evolves. The critical value is achieved when the perturbation neither grows neither decays, so the critical value will be achieved when the growth rate (3.1) becomes 0. Following the $\alpha = 2$ case, the second term of the growth rate becomes after integration

$$\hat{v}(k) = -\int_{-\infty}^{\infty} e^{-|x|^2} e^{-ikx} dx = -\sqrt{\pi} e^{-\frac{k^2}{4}}. \tag{3.5}$$

In order to guarantee that $\lambda(k)$ is always negative or zero, we find the most negative value of $\hat{v}(k)$ which is $\partial_k \sqrt{\pi} e^{-\frac{k^2}{4}} \Big|_{k=k_c} = -\frac{1}{2} e^{-\frac{k_c^2}{4}} k_c = 0$; so $k_c = 0$. If $\lambda \leq 0$ for $k = k_c$, then $\lambda \leq 0$ for any other value of k. Now we can obtain the critical value of the diffusion coefficient by imposing

the condition $\lambda(k = k_c) = 0$

$$\lambda(k_c) = 0 \longrightarrow \tilde{D}_c = -\hat{v}(k_c) \tag{3.6}$$

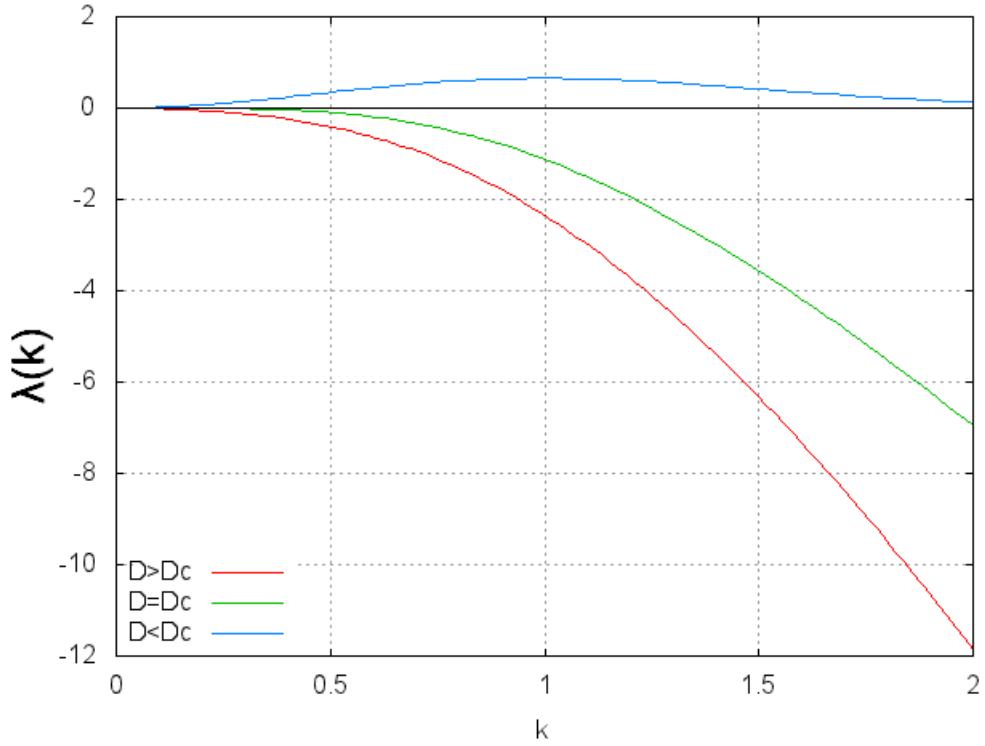

Figure 3.3: Growth rate $\lambda(k)$ of the perturbation for different values of $\tilde{D}$ in the $\alpha = 2$ case. The value of $\lambda(k)$ is shown in the y-axis while x-axis is k.

Since $k_c = 0$, evaluating at (3.5) we obtain $\hat{v}(k_c) = -\sqrt{\pi}$ and then

$$\tilde{D}_c = \sqrt{\pi}. \tag{3.7}$$

Returning to unscaled units we have $\frac{D_c}{\epsilon\rho_0 R} = \sqrt{\pi}$. From here, we can isolate the critical value of D_c for $\alpha = 2$

$$D_c = \sqrt{\pi}\rho_0\epsilon R \tag{3.8}$$

In a more general case, for an arbitrary α we can compute the value of the Fourier transform at the critical wave number $k_c = 0$. We can obtain an analytical solution[1] if we define the Gamma

[1] Knowing that GEM-α is a family of even functions and making the change of variable $x^\alpha = u$.

function as $\Gamma(z) = \int_0^\infty x^{z-1}e^{-x}dx$.

$$\hat{v}(k=0) = -\int_{-\infty}^{\infty} e^{-|x|^\alpha}dx = -2\Gamma\left(\frac{\alpha+1}{\alpha}\right). \tag{3.9}$$

Some critical values are reflected in Table 3.1. Finally, if we turn back to dimensional variables $\tilde{D}_c = \frac{D_c}{\epsilon\rho_0 R}$, for any value of α the critical value of the diffusion coefficient will be determined by

$$D_c = 2\Gamma\left(\frac{\alpha+1}{\alpha}\right)\epsilon\rho_0 R. \tag{3.10}$$

As we can see this relationship could be reformulated in order to obtain ϵ_c easily. (3.10) gives us the critical point when any change on the system or potential parameters will lead to two different regimes: either clusters are formed either the particles will be randomly distributed.

Table 3.1: Values of D_c computed as the Fourier transform of the dimensionless potential $\tilde{v}(\tilde{x}) = \frac{v(x)}{\epsilon}$.

α	$\tilde{D}_c = -\tilde{v}(k_c = 0)$
1	$2\Gamma(2) = 2$
2	$2\Gamma\left(\frac{3}{2}\right) = \sqrt{\pi} \approx 1.77245$
3	$2\Gamma\left(\frac{4}{3}\right) \approx 1.78596$
4	$2\Gamma\left(\frac{5}{4}\right) \approx 1.81280$
5	$2\Gamma\left(\frac{6}{5}\right) \approx 1.83634$
6	$2\Gamma\left(\frac{7}{6}\right) \approx 1.85544$
7	$2\Gamma\left(\frac{8}{7}\right) \approx 1.87088$

We will check numerically in Section 4.3 the result for $\alpha = 2$ obtained in (3.7).

Note that the critical value of k is $k_c = 0$. When $D > D_c$ the maximum of the growth rate is at $k > k_c >$, as seen in Fig. 3.3.

Chapter 4

Cluster properties

As we have seen in Section 3.1, from random initial conditions and with a GEM-α attractive potential, after a certain time we can consider the clusters generated as an isolated system since they only collapse at a very long times. From here we will set the particles at the neighbourhood of a certain point of the x-axis as an initial condition, so an unique cluster is formed and we don't have to wait for the collapse of all the particles.

We will focus on three characteristics of the cluster: (1) its effective diffusion coefficient and the depence on the particles own diffusion, (2) the size of the generated cluster and (3) the critical value that leads to a cluster formation. When possible, an analytical justification will be made.

4.1 Cluster diffusion coefficient

Einstein's formulation stands that the diffusion coefficient of a Brownian particle is related to the mean squared displacement $\langle x^2 \rangle$. As seen in previous studies [17], an aggregation of Brownian particles could be considered as a Brownian particle itself. Considering an isolated Brownian particle in 1-dimension, its diffusion coefficient D is defined as

$$\langle [x(t) - x(0)]^2 \rangle = 2D(t)\,t. \tag{4.1}$$

If we arrange an assembly of particles we can always define the spatial evolution of its center of mass as

$$x_{CM}(t) = \frac{1}{N}\sum_{i=1}^{N} x_i(t). \tag{4.2}$$

Computing the derivative of the x_{CM} position we can recall (2.4)

$$\frac{dx_{CM}}{dt} = \frac{1}{N}\sum_{i=1}^{N} \dot{x}_i(t) = \frac{1}{N}\sum_{i=1}^{N}\left(-\sum_{j=1}^{N} \nabla v(x_i - x_j) + \sqrt{2D}\xi_i(t)\right). \tag{4.3}$$

If our interaction satisfies the Newton's 3^{rd} law, the force applied by i over j will be the same as the one done by j over i but for the sign, $\nabla_i v(x_i - x_j) = -\nabla_i v(x_j - x_i)$. Simplifying the right-hand side of the equation and applying the Gaussian noise properties (2.3) and (2.2) we obtain

$$\langle [x_{CM}(t) - x_{CM}(0)]^2 \rangle = \frac{2Dt}{N}, \tag{4.4}$$

so the diffusion coefficient of the cluster $D_{cluster}$ can be defined as a function of D and N

$$D_{cluster} = \frac{D}{N} \tag{4.5}$$

being N the number of the particles that form the cluster. As expected, $D_{cluster}$ will be always smaller than D since it is the result of averaging the fluctuations of the individual Brownian particles that form the cluster.

Fig. 4.1 shows the time evolution of a cluster with its center of mass computed at each temporal step. Our goal is to compute the diffusion of the center of mass and prove that follows the relationship set in (4.5).

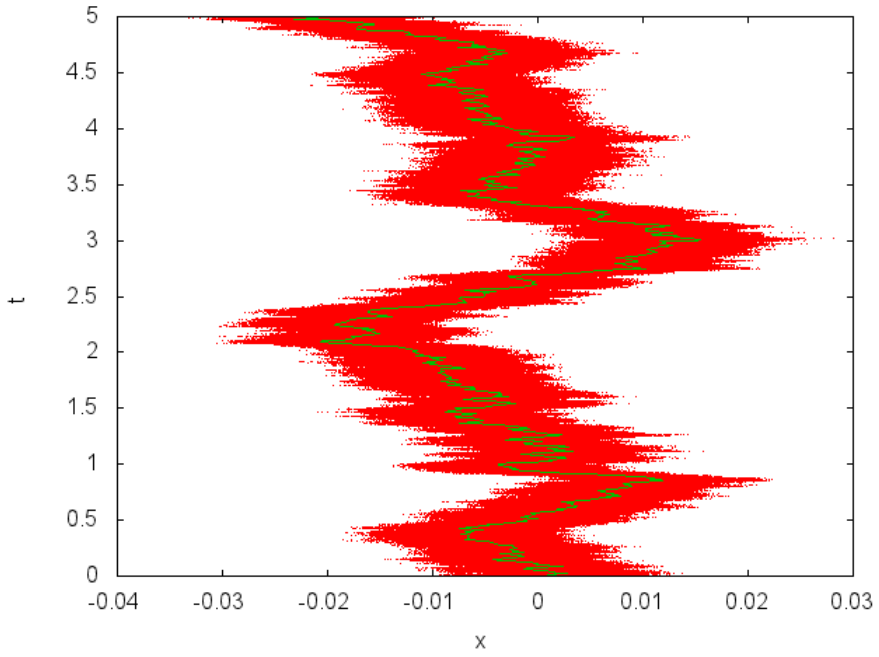

Figure 4.1: Temporal evolution of a cluster of 50 particles (red) with $D = 4 \times 10^{-3}$ and the trajectory of the computed center of mass for each time (green). Time evolution is shown in y-axis while x-axis is the spatial variable. $R = 0.1$, $\epsilon = -0.3$ and $\alpha = 2$. System size is $L = 1$ but a zoom-in is made in order to clearly show the evolution of the center of mass.

We want to determine the diffusion coefficient of the cluster, so we follow same way used to compute the diffusion coefficient for an individual particle. In order to achieve a good approximation to the theoretical value we need to average different trajectories and compute the square of the displacement of the cluster's center of mass. After that, we can consider the center of mass as an individual Brownian particle and apply (4.1). We compute $D_{cluster}$ for one cluster in Figs. 4.2 and 4.3.

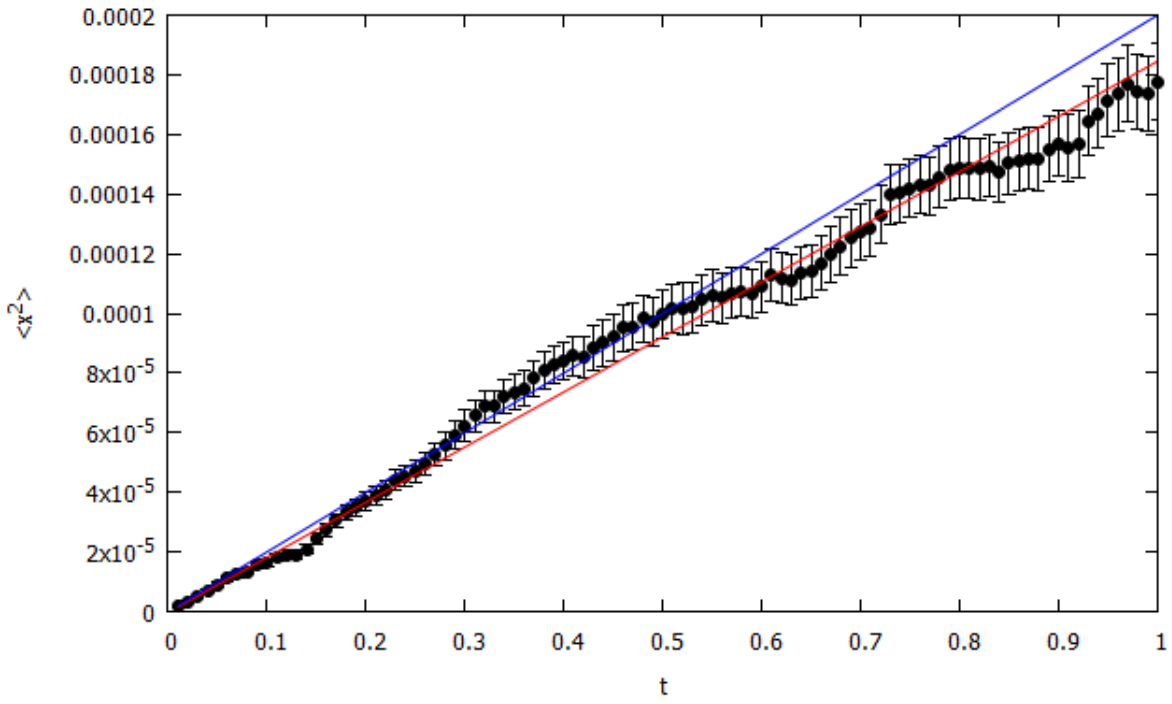

Figure 4.2: $\langle x^2_{CM} \rangle$ versus time with $D = 5 \times 10^{-3}$, $N = 50$ and 300 averaged cluster realizations. $\epsilon = -0.3$, $R = 0.1$, red line is a weighted linear fit that gives $D_{cluster} = (0.924 \pm 0.007) \times 10^{-4}$. Green line is the theoretical value $D_{cluster} = 1 \times 10^{-4}$ computed using (4.5). Error bars are the standard deviations of the mean over clusters.

For Fig. 4.2 we used a smaller number of particles per cluster but a larger number of clusters averaged than in Fig. 4.3. As we can see the larger amount of realizations done lead to a smaller relative error in the computed $D_{cluster}$ and a more approximated value compared to the theoretical one predicted by (4.5).

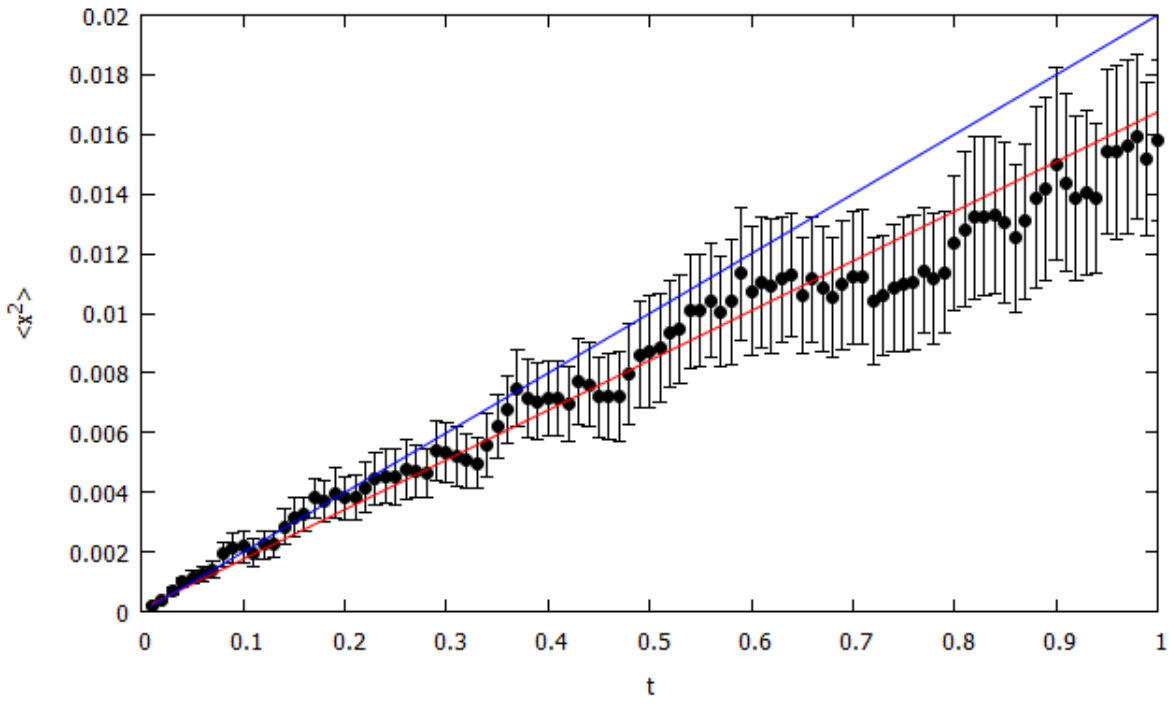

Figure 4.3: Same as Fig. 4.2 but with $D = 1$, $N = 100$ and 50 averaged trajectories. Computed $D_{cluster} = 0.0083 \pm 0.0003$. Theoretical value is $D_{cluster} = 0.01$.

On the other hand, the formula (4.5) only depends on the number of particles N and the particle diffusion coefficient D. In order to check that $D_{cluster}$ is independent of ϵ and R, providing that the cluster is formed, we run the simulation as done in Fig. 4.2 but changing those parameters. Results are shown in Fig. 4.4.

As we can see, a change on the parameters does not imply a monotomic change on $D_{cluster}$: the computed diffusion coefficient fluctuates around a mean value but those fluctuations are, in the worst case, of a 0.2% of the computed value. Computing the standard deviation of each value, we can observe that almost all the values are compatible with the $D_{cluster}$ given at Fig. 4.2. On the other hand the extreme fluctuations are incompatible between them in terms of error, for example in Fig. 4.2a the value computed for $\epsilon = -5$ does not agree with the one for $\epsilon = -10$; similar situation for Fig. 4.2. While the results coincide in the order of magnitude with the theoretical values, the fact of not having a value included in all of the error ranges warns us that perhaps the number of trajectories used to averaging is not enough or the way that boundary conditions are implemented in the computer code should be improved.

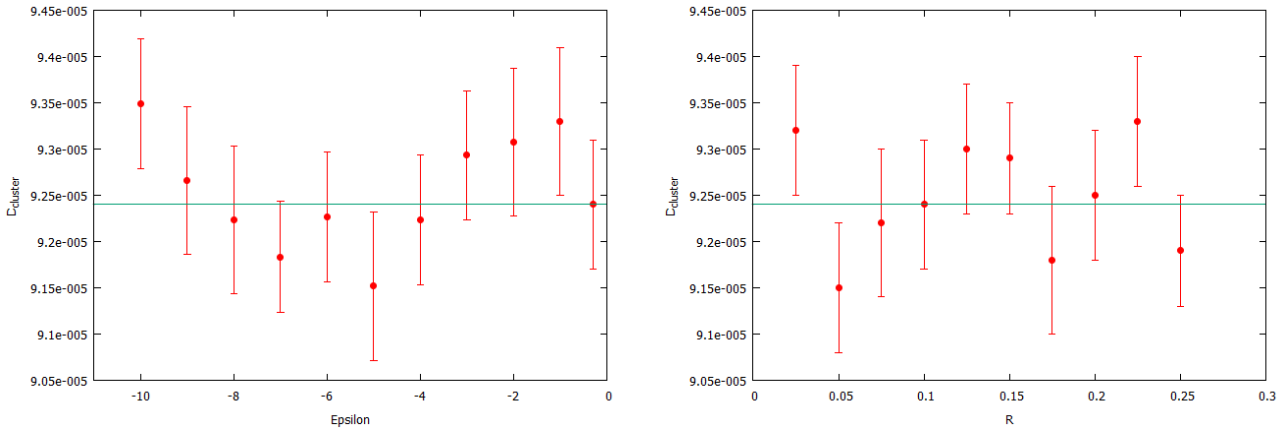

(a) (b)

Figure 4.4: Computed value of $D_{cluster}$ in the y-axis versus (a) ϵ and (b) R. Same parameters as Fig. 4.2 except for (a) ϵ and (b) R. Blue line is $D_{cluster} = (0.924 \pm 0.007) \times 10^{-4}$ obtained in Fig. 4.2. Error bars are the standard deviation of the mean of the clusters.

4.2 Size of the cluster

Once we have proved that the only parameters that have an impact on $D_{cluster}$ are N and D, we can ask ourselves which role play the other parameters in the cluster dynamics. As commented before, the number of clusters formed at a certain time is observed to grow as α increases. Providing that the number of particles is constant. This means that the averaged number of particles at each cluster decreases as α gets larger. It is obvious to think that the number of particles will affect the size of the cluster, but we will focus on determining the dependences of the cluster size with D and α for constant N.

4.2.1 Theoretical description

Using the Dean-Kawasaki presented in (2.6) we will study analitically the size of the cluster. In order to relieve the notation we will drop the tilde. We consider the steady state solutions with zero flux, $J = 0$, so

$$\rho(x) \int dx' \nabla v(x - x') \rho(x') = -D \nabla \rho(x), \tag{4.6}$$

which, after integration, turns into

$$\rho(x) = \exp\left[\frac{1}{D}\left(\mu - \int dx' \rho(x') v(x - x')\right)\right], \tag{4.7}$$

being μ an integration constant that can be identified as the chemical potential.

We proceed as an iterative procedure by substituting in Eq. (4.7) a density approximation in order to obtain an improved one. Considering the case $D \approx 0$ (no thermal noise) in the one-dimensional scenario the density of clusters become an arrangement of delta-functions

$$\rho(x') \approx N_p \sum_n \delta(x' - nc), \tag{4.8}$$

where N_p is the number of particles, n the index of the clusters, and c the distance between clusters. We can consider an isolated cluster, so Eq. (4.8) becomes

$$\rho(x') \approx N_p \delta(x'), \tag{4.9}$$

integrating the density of Eq. (4.7) we obtain

$$\rho(x) \approx \exp\left[\frac{1}{D}\left(\mu - N_p v(x)\right)\right], \tag{4.10}$$

being the potential Eq. (2.5) in normalized parameters

$$v(x) = -\exp\left(-|x|^\alpha\right). \tag{4.11}$$

Equation (4.10) is an improved approximation fot cluster density valid for small values of D. Our first approximation was a delta-function at $x = 0$, so there will be the maximum density. Considering that the first iteration smooths the density distribution, we define the width of the cluster as the width of the density distribution at half the maximum. So, the maximum of density will be located at $x \approx 0$,

$$\rho_{max} = \rho(0), \tag{4.12}$$

where x_s the half width of the cluster, the middle of the distribution is located at $\rho(x_s) = 0.5\rho(0)$,

$$\exp\left(\frac{1}{D}\left[\mu + N_p exp\left(-|x_s|^{\alpha}\right)\right]\right) = \frac{1}{2} exp\left(\frac{1}{D}(\mu + N_p)\right) \tag{4.13}$$

since $v(0) = 1$. Isolating the exponential we obtain

$$1 - \frac{D}{N_p} ln(2) = \exp\left(-|x_s|^{\alpha}\right). \tag{4.14}$$

Taking logarithms and recalling the equation (4.10) is valid only for small D so

$$|x_s|^{\alpha} = -ln\left(1 - ln(2)\frac{D}{N_p}\right) \approx ln(2)\frac{D}{N_p}. \tag{4.15}$$

The width of the cluster will be $S = 2|x_s|$, and finally we obtain the relation

$$S \propto D^{\frac{1}{\alpha}}. \tag{4.16}$$

As expected, the size of the cluster decreases as α increases. The mechanism behind this relation could be the fact that for smaller α the tail of the potential's profile grows, increasing its range of action an allowing the formation of a spreaded cluster of particles. The increasing dependece of size on D is easier to understand: diffusion spreads the cluster. Note that we were working in scaled units, so the true relation is

$$\frac{S}{R} \propto D^{\frac{1}{\alpha}} \tag{4.17}$$

so S will increase linearly with R.

4.2.2 Numerical validation

In order to validate numerically the relation (4.16) we divide the 1-dimensional space in cells with size $\ll L$. At each time we recenter the ensemble of particles so the center of mass will be always at $x = 0$. Once we reach the stationary behaviour of the cluster, at every time step we count the number of particles inside each cell. We repeat the same process until the simulation

ends and we generate an histogram. As before, the size of the cluster is defined as the width of the histogram at half of the height. An example is shown in Fig. 4.5a.

We compute the average size for 10^4 time steps with different diffusion coefficient D for each value of α. We fit a linear function in order to study its dependence in Fig. 4.5b for $\alpha = 2$.

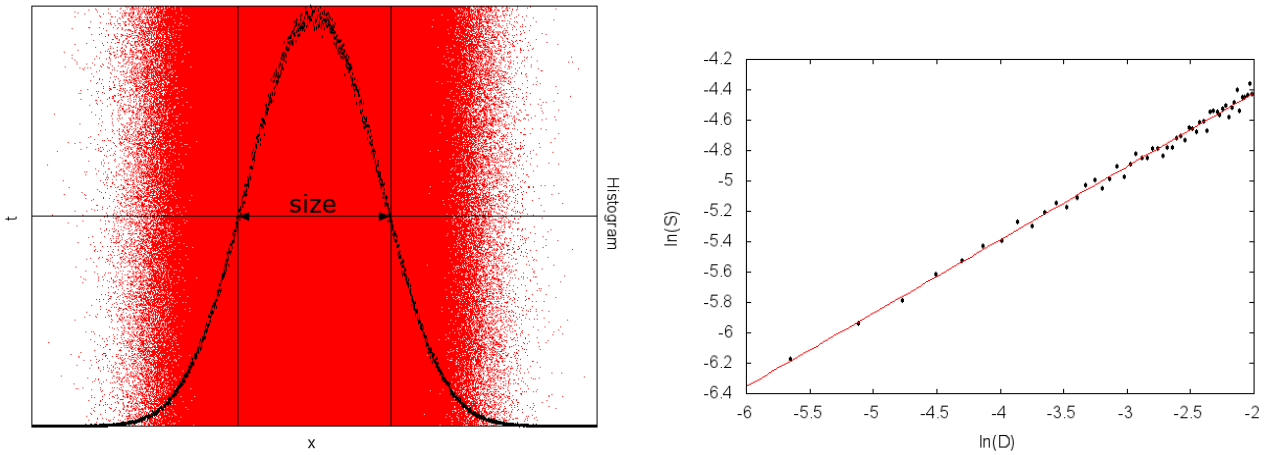

(a) (b)

Figure 4.5: (a) Example of the method used for the size calculation. S is defined as the width of the density histogram at half of its maximum value. Note that the center of mass is displaced in order to be always at the same $x = 0$. (b) Log of the size S of the clusters generated for 300 particles versus the log of the diffusion coefficient D (black dots) for $\alpha = 2$. $\epsilon = -0.3$. A linear fit is done (red line). $ln(S) = -(3.45 \pm 0.02) + (0.483 \pm 0.006) ln(D)$, equivalent to $S = KD^B$.Correlation coefficient given is $r^2 = 0.923$.

Now that we have observed a dependence of S on D we repeat the same analysis for different values of α in order to check the relation (4.16). Size as a function of D is computed for $\alpha \in [3,6]$ and shown in Figs. 4.6.

As we can see the results are pretty similar for all the cases; size increases as the diffusion coefficient does. Once we have the function $S(D) = KD^B$ for some values of α we can check (4.16). $\frac{1}{B}$ versus α is plotted in Fig. 4.7; we compare the size of the cluster for a fixed D.

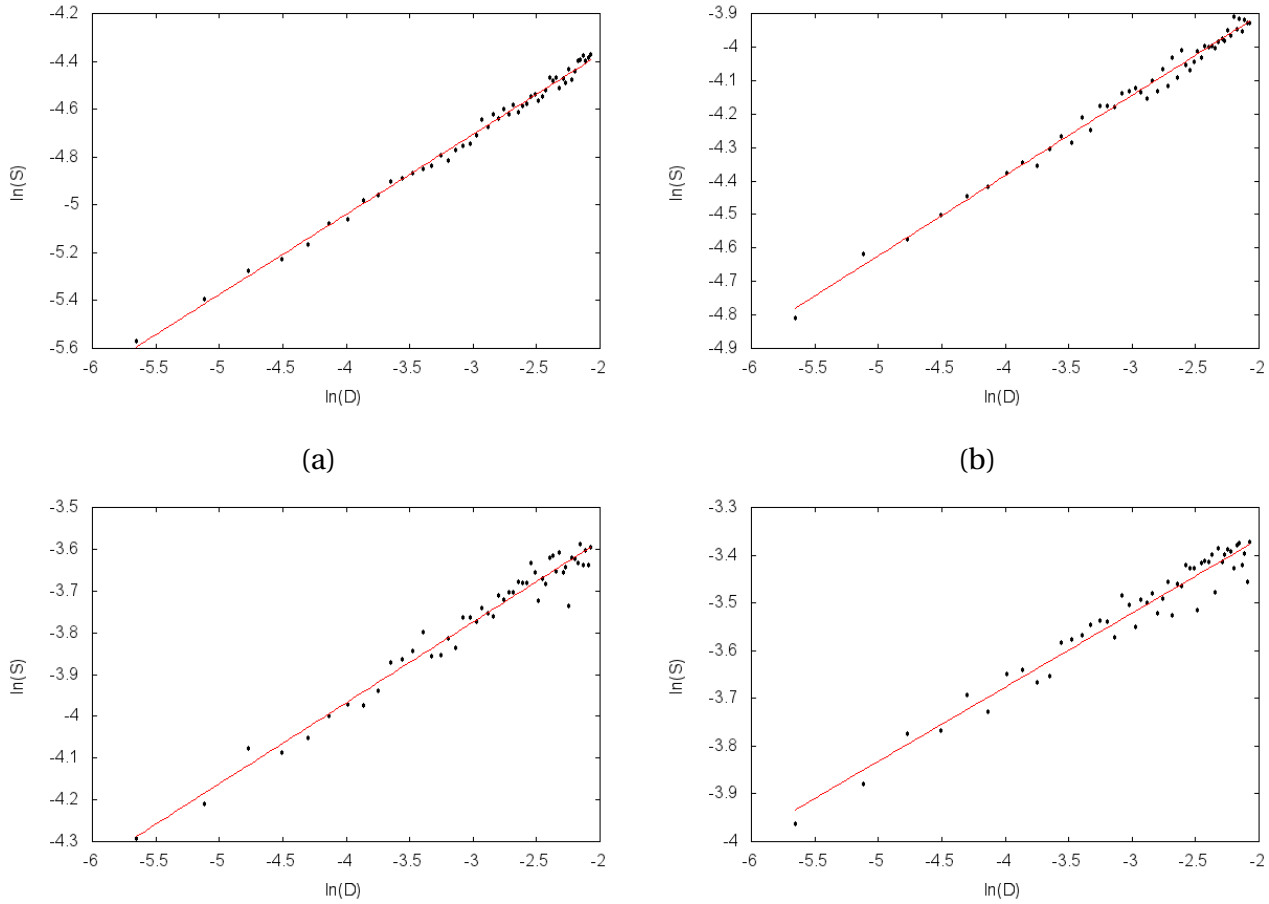

Figure 4.6: Same as Fig. 4.5b for different values of α. A fit with the form $S(D) = KD^B$ is done (red line). (a) $\alpha = 3$. $ln(S) = (-3.70 \pm 0.01) + (0.335 \pm 0.004) ln(D)$; .934; (b) $\alpha = 4$. $ln(S) = (-3.43 \pm 0.01) + (0.240 \pm 0.004) ln(D)$; $r^2 = 0.924$; (c) $\alpha = 5$. $ln(S) = (-3.19 \pm 0.02) + (0.194 \pm 0.005) ln(D)$; $r^2 = 0.938$; (d) $\alpha = 6$. $ln(S) = (-3.06 \pm 0.02) + (0.155 \pm 0.005) ln(D)$; $r^2 = 0.927$.

As expected, for a fixed value of α the size of the cluster increases as D does; the particles will tend to diffuse more and break the cluster. For smaller values of D the attractive force wins the diffusion and the Brownian walkers will be at a higher local density.

Theoretical result says that $\frac{1}{B} = \alpha$. We can see that the coefficient given by the linear fit 0.98 ± 0.02 is fully compatible with this. As expected, the size of the clusters increases as D does and decreases as α grows.

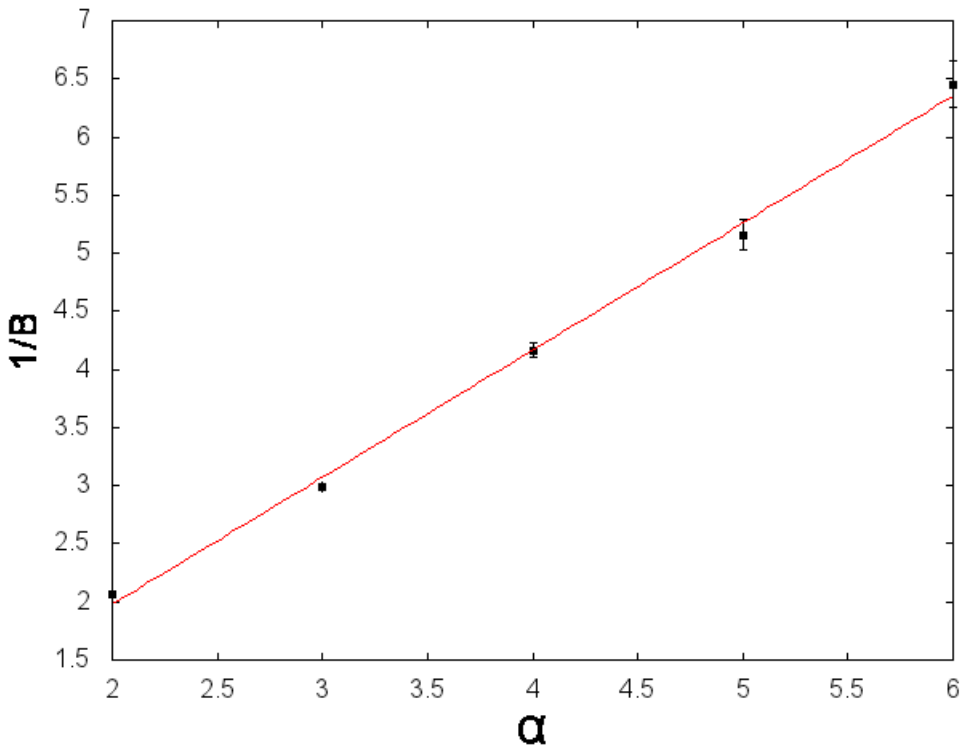

Figure 4.7: Dependence of $\frac{1}{B} \propto \alpha$. A fit is done (red line). $\frac{1}{B(\alpha)} = -(0.004 \pm 0.009) + (0.98 \pm 0.02)\alpha$; $r^2 = 0.86$

4.3 Critical point for cluster formation

Our $GEM - \alpha$ attractive potential is very robust in the cluster formation. Since the interaction is always attractive the particles tend to coalesce only stopped by the diffusion. We will inspect two equivalent possibilities to cross a transition from cluster formation cluster destruction: (1) the cluster will not be formed if the diffusion is large enough to win the attraction term, (2) the strength of the attraction is not large enough to mantain the particles together and the cluster breaks up.

We want to check if the stability analysis done previously in Section 3.2 of the critical point of cluster reproduces the transition from clustering to no-clustering situation. We will simulate the case for $\alpha = 2$ in order to check the theoretical value (3.10). Computing $\Gamma\left(\frac{3}{2}\right) = \sqrt{\pi}$, the growth rate (3.1) will be zero if $\tilde{D}_c = \sqrt{\pi} = \frac{D_c}{\rho_0 \epsilon R}$. The relationship between the parameters of the systems at the critical point will be

$$D_c = \sqrt{\pi}\epsilon\rho_0 R. \tag{4.18}$$

We will check the theoretical value both for the diffusion coefficient D_c and the magnitude of the potential ϵ.

Now the particles will be initially distributed in a small region at $x = 0$ since we will compare the result of this simulation with the theoretical framework of Section 3.2 in which an homogeneous initial condition is assumed. That initial condition will guarantee that only one cluster will be formed. The algorithm detects the presence of a cluster in a very similar way to the method used in the size calculation: the space is divided in small cells and we compute the number of particles inside each cell at every time step. After that, we compute the maximum and the minimum values of normalized density for each cell. When the maximum and the minimum density values are equal to 1 the particles are equally distributed along the system length. On the other hand if the minimum value is close to 0 (and the maximum is larger than 1) a cluster is formed.

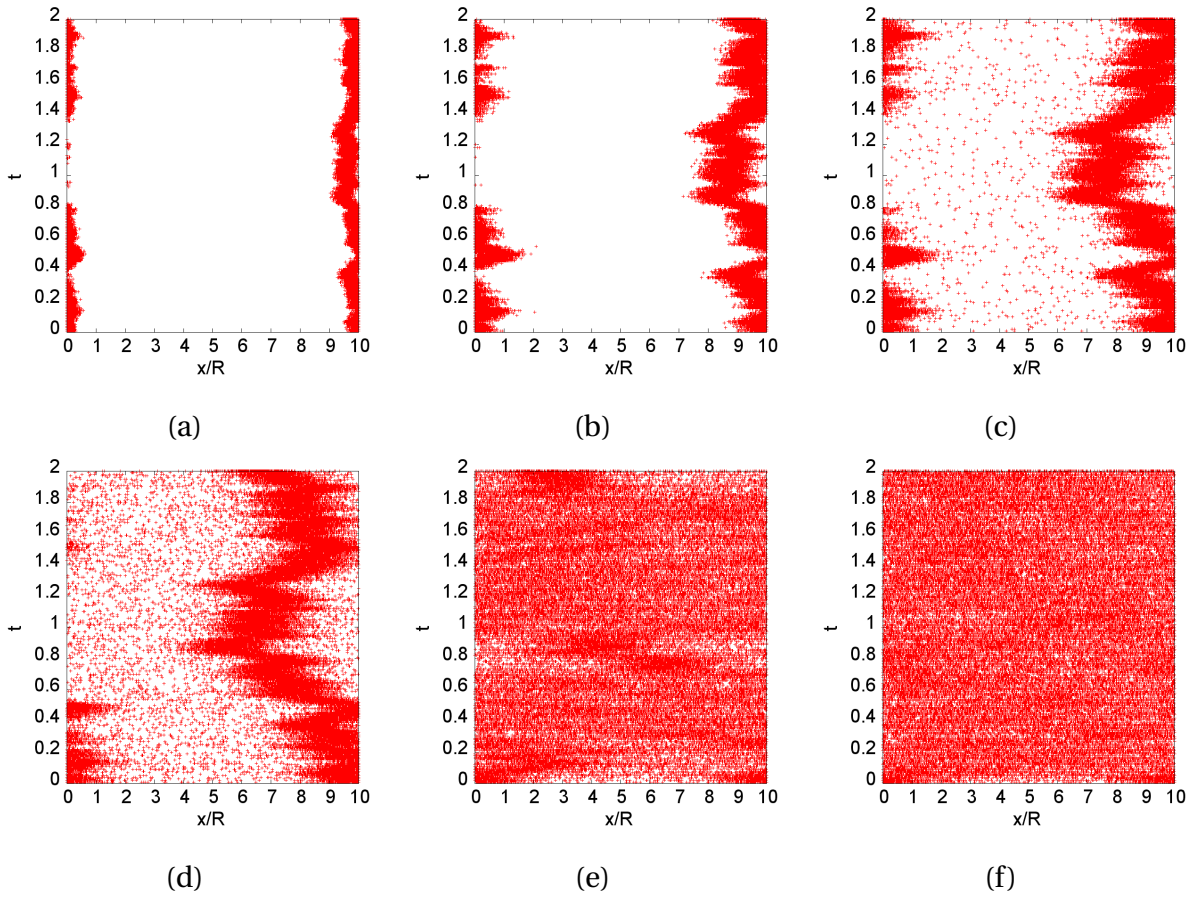

Figure 4.8: Trajectories for $\rho = 300$, $\epsilon = -0.3$, $R = 0.1$, $\alpha = 2$. The time evolution is shown in y-axis while x-axis is the spatial coordinate. (a) D=0.5, (b) D=5, (c) D=10, (d) D=13, (e) D=15, (f) D=16.

Example trajectories computed are shown in Fig. 4.8. As we can see, for $D = 13$ the cluster is clearly formed while for $D = 16$ the cluster is not observed. We guess that the criticial value will be around $D = 15$.

We plot the averaged maximum and minimum value of the density for simulations with different D in Fig. 4.9.

As we can see there is a region of change around the theoretical value D_c: starting from $D = 12$ as its value increases the difference between the maximum and the minimum density decreases. This means that the cluster spreads out and the particles are more equally distributed, as seen in the discussion for the cluster size.

Once $D \approx 16$ the maximum and minimum density values are close to 1, meaning that the particles are distributed all over the system's size, i.e. the cluster is broken. It's hard to identify

a numerical value for the critical value but if we compare the theoretical D_c we can see that fits the behaviour reflected by our simulation.

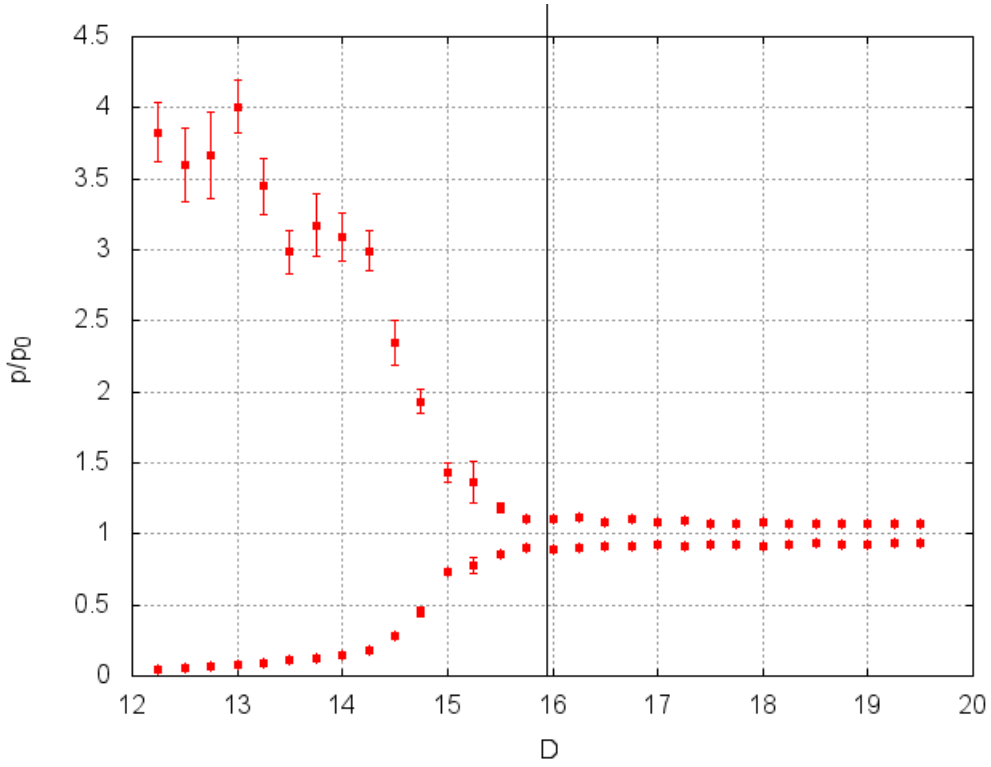

Figure 4.9: We compute the maximum and the minimum normalized spatial density (y-axis) for the simulation at each value of D (x-axis). $\alpha = 2$, and same parameters as Fig. 4.8. 10 simulations were done to compute each pair of points. Theroretical value is computed using the Eq. (3.8), $D_c = 15.95$, plotted as a black vertical line.

We do the same analysis for ϵ. Results are shown in Fig. 4.10. Discussion is analogous to the previous one: the maximum and minimum value gets closer as $|\epsilon|$ decreases. As expected the cluster breaks up when the magnitude of the potential is weak enough to be surpassed by the diffusion of the particles.

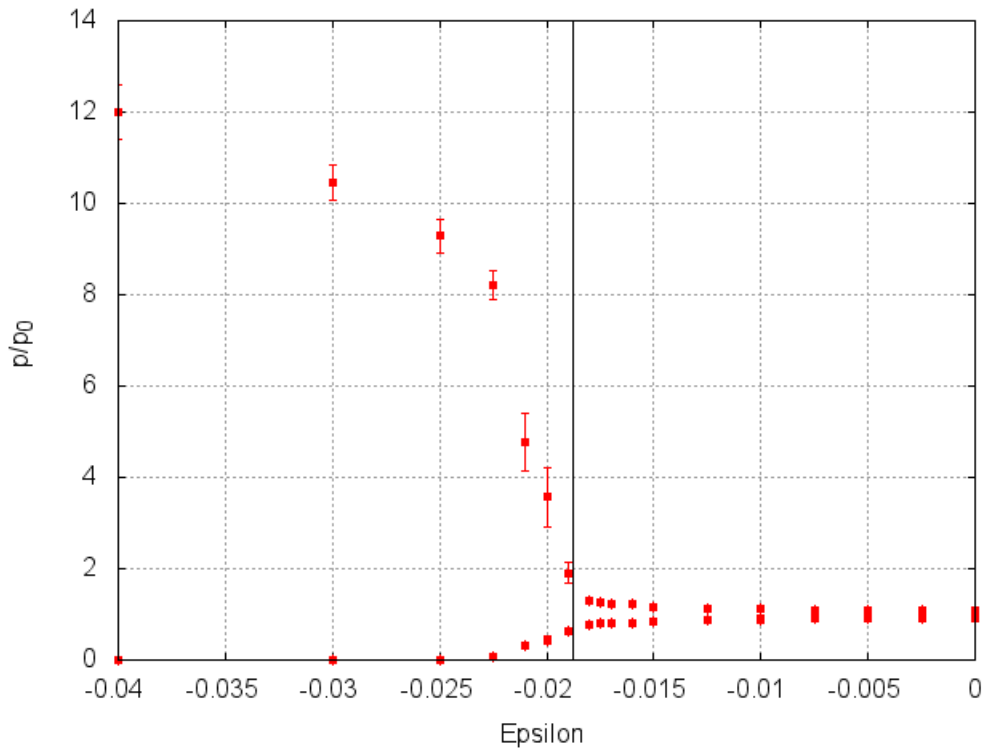

Figure 4.10: We compute the maximum and the minimum normalized spatial density (y-axis) for the simulation at each value of ϵ (x-axis). Same parameters as Fig. 4.9 with $D = 1$. Theroretical value is computed using the Eq. (3.8), $\epsilon_c = -0.0188$, plotted as a black vertical line.

As we can see, both in Figs. 4.9 and 4.10 the numerical values looks a little displaced from the theoretical one. This could be explained by the dimensionality of the systems: the aren't phase transitions at 1d in the presence of noise; the change of behaviour is smooth. This adds a difficulty on determining the critical values for numerical simulations in 1d systems.

For completeness we plot different trajectories both for cases where the cluster is formed and where the attraction is not enough. We want to see if the initial condition plays a role on the determination of D_c by setting the initial conditions or as a cluster or as a uniform distribution. Linear stability works for the uniform distribution case but as we can see the critical value fit approximately the behaviour observed for the case in which we start the simulation with the cluster formed. For $\epsilon = -0.019$ ($|\epsilon| < \epsilon_c$) the cluster is clearly formed if the particles are setted at a small region but barely detectable for uniform initial condition. On the other hand for $\epsilon = -0.018$ the cluster dissapears for both cases. This suggests that the critical value may

have a weak dependence on the initial distribution of particles but this difference is very small (a change between -0.018 and -0.019) and of the order of the error of precision in Fig. 4.10, i.e. the initial condition does no determine the transition point.

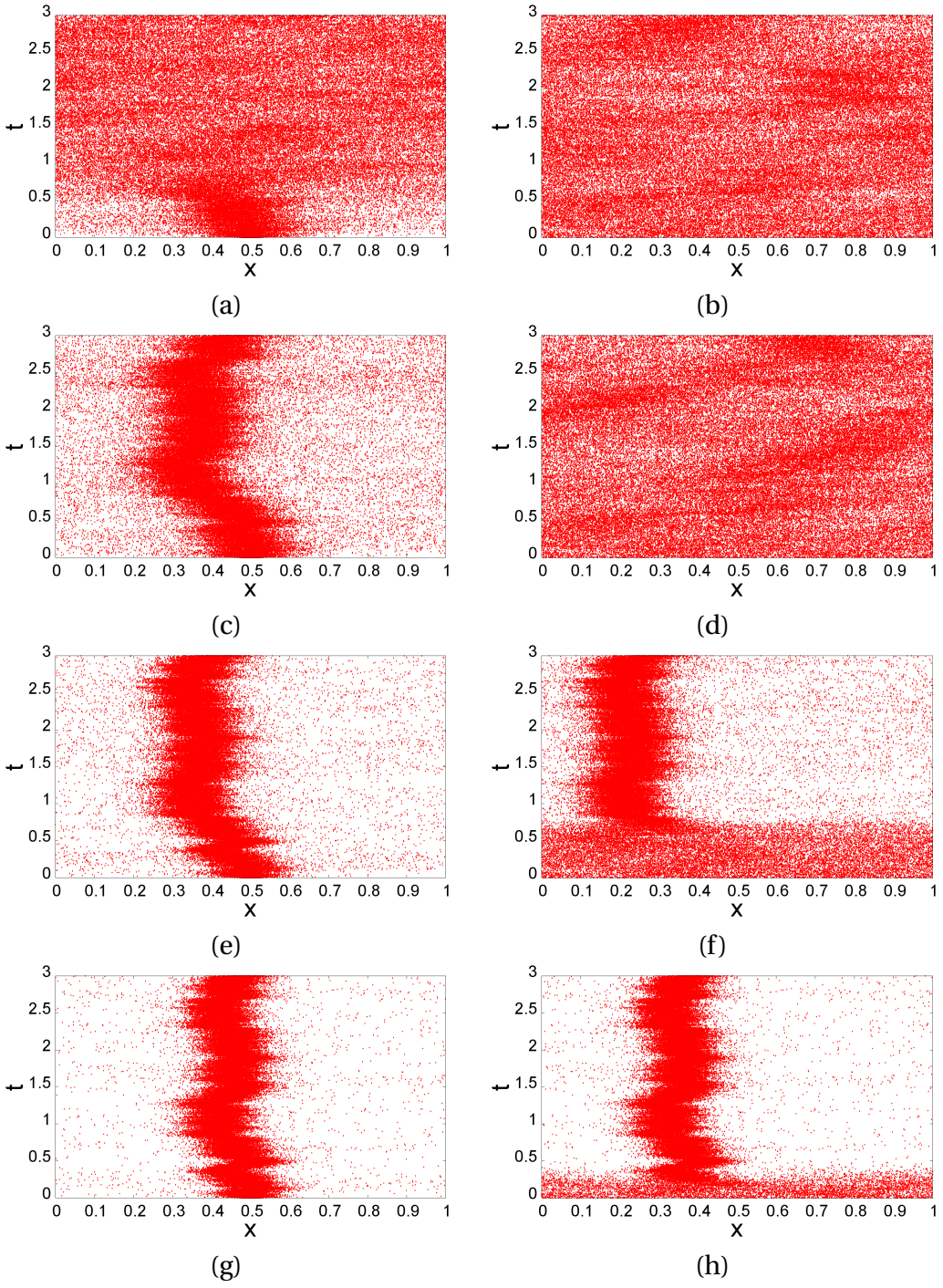

Figure 4.11: Time evolution shown in y-axis of the spatial distribution of the cluster shown in x-axis. $D = 1$, $N = 300$, $R = 0.1$, (a) and (b) $\epsilon = -0.018$, (c) and (d) $\epsilon = -0.019$, (e) and (f) $\epsilon = -0.021$, (g) and (h) $\epsilon = -0.025$. Simulations (a), (c), (e) and (g) starts with the particles placed at a small area near to $x = \frac{L}{2}$; (b), (d), (f) and (h) simulations are done with initial random positions.

Chapter 5

Summary and further work

We have studied the dynamics of Brownian particles with soft-core attractive two-body interactions. We have set a GEM-α family of potentials modulated by the parameter α that changes its profile. We have seen how initially the particles tend to form separated clusters whose center of mass behaves as a Brownian particle itself. Those clusters tend to collapse in a unique cluster formed by all the assembly of the particles at a very long time, so we have focused our study on a isolated cluster. The soft-core attracting Brownian particles form a cluster with a diffusion coefficient that only depends on the particle properties such as the diffusion coefficient of the individual particles and the number of particles that form the cluster. On the other hand, the cluster diffusion coefficient is proved to be fully independent of the potential parameters. We have also studied the Dean-Kawasaki equation of this system and how the size of the cluster is determined both by the potential profile and the diffusion coefficient. We have also performed a linear stability analysis that allowed us to study the cluster formation conditions, finding the critical point for cluster formation for any attractive GEM-α potential. Finally, we have seen how the initial condition (cluster already formed or uniform distribution) seems irrelevant in order to determine that transition point.

The next logical step in our study will be the 2d and 3d cases in order to check its applicability, like the Collembola aggregation, since real 1d systems are not abundant. Some results, such as the cluster diffusion coefficient, can be easily generalized for higher dimensions, but others should require a deeper study. Another possible further work could be the study of the evolution of the number of clusters. As we have seen, initially a number of clusters were formed but

they tend to collapse as time passes, ending in a unique large at extremely long times; the study of how the number decreases as a function of time could be a field of interest. Changing the potential applied could be another logical step; potentials that go as R^{-1} (being R the distance between particles) are common in nature like the gravitational potential.

Bibliography

[1] Albert Einstein. On the movement of small particles suspended in stationary liquids required by the molecular-kinetic theory of heat. *Annalen der Physik*, 17:549–560, 1905.

[2] Ronald F. Fox. Rectified Brownian movement in molecular and cell biology. *Phys. Rev. E*, 57:2177–2203, Feb 1998.

[3] Emilio Hernández-García and Cristóbal López. Birth, death and diffusion of interacting particles. *Journal of Physics: Condensed Matter*, 17(49).

[4] Frank Schweitzer. *Brownian Agents and Active Particles: Collective Dynamics in the Natural and Social Sciences*. Springer Science & Business Media, 1 edition, 2007.

[5] Emilio Hernández-García, Els Heinsalu, and Cristóbal López. Spatial patterns of competing random walkers. *Ecological Complexity*, 21:166 – 176, 2015.

[6] Jean-Baptiste Delfau, Hélène Ollivier, Cristóbal López, Bernd Blasius, and Emilio Hernández-García. Pattern formation with repulsive soft-core interactions: discrete particle dynamics and Dean-Kawasaki equation. *Physical Review E*, 94:1–13, 2016.

[7] D. S. Dean. Langevin equation for the density of a system of interacting Langevin processes. *Journal of Physics Physics A: Mathematical and General*, 29(24):L613.

[8] Stephen P. Hopkin. *Biology of the Springtails: (Insecta: Collembola)*. OUP Oxford, 1 edition, 197.

[9] M. B. Usher and Mary Hider. Studies on populations of Folsomia candida (insecta: Collembola): causes of aggregation. *Pedobiologia*, 15:276–283, 1975.

[10] M. B. Usher. Some properties of the aggregations of soil arthropods: Collembola. *Journal of Animal Ecology*, 3:607–622, 1969.

[11] Ken A. Dill and Sarina Bromberg. *Molecular Driving Forces: Statistical Thermodynamics in Chemistry and Biology*. Garaland Science, 3 edition, 2003.

[12] Bianca M. Mladek, Dieter Gottwald, Gerhard Kahl, Martin Neumann, and Christos N. Likos. Formation of polymorphic cluster phases for a class of models of purely repulsive soft spheres. *Phys. Rev. Lett.*, 96:045701, Jan 2006.

[13] Christos N. Likos. Why do ultrasoft repulsive particles cluster and crystallize? analytical results from density-functional theory. *The Journal of Chemical Physics*, 126:224502, Jun 2007.

[14] K. Kawasaki. Stochastic model of slow dynamics in supercooled liquids and dense colloidal suspensions. *Physica A: Statistical Mechanics and its Applications*, 208:35–64, 1994.

[15] Raúl Toral and Colet Pere. *Stochastic Numerical Methods. An Introduction for Students and Scientists*. Wiley-VCH, 1 edition, 2014.

[16] Box G. E. P. and Mervin E. Muller. A note on the generation of random normal deviates. *Ann. Math. Statist.*, 29:610–611, 1958.

[17] S. Sabel'ev, Fabio Marchesoni, A. Taloni, and F. Nori. Diffusion of interacting Brownian particles: Jamming and anomalous diffusion. *Phys. Rev. E*, 74:021119, 2006.